https://doi.org/10.5194/gmd-2020-130
Preprint. Discussion started: 10 July 2020

Geoscientific Model Development Discussions

CrocO_v1.0 : a Particle Filter to assimilate snowpack observations in a spatialised framework

Bertrand Cluzet[1], Matthieu Lafaysse[1], Emmanuel Cosme[2], Clément Albergel[3], Louis-François Meunier[3], and Marie Dumont[1]

[1]Univ. Grenoble Alpes, Université de Toulouse, Météo-France, CNRS, Centre d'Études de la Neige, Grenoble, France
[2]Institut des Géosciences de l'Environnement, IGE, UGA-CNRS, Grenoble, France
[3]CNRM, Université de Toulouse, Météo-France, CNRS, 31057 Toulouse, France.

Correspondence: Bertrand Cluzet (bertrand.cluzet@meteo.fr)

Abstract. Monitoring the evolution of the snowpack properties in mountainous areas is crucial for avalanche hazard forecasting and water resources management. In-situ and remotely sensed observations provide precious information on the snowpack but usually offer a limited spatio-temporal coverage of bulk or surface variables only. In particular, visible-near infrared (VIS-NIR) reflectance observations can inform on the snowpack surface properties but are limited by terrain shading and clouds. Snowpack modelling enables to estimate any physical variable, virtually anywhere, but is affected by large errors and uncertainties. Data assimilation offers a way to combine both sources of information, and to propagate information from observed areas to non observed areas. Here, we present CrocO, (Crocus-Observations) an ensemble data assimilation system able to ingest any snowpack observation (applied as a first step to the height of snow (HS) and VIS-NIR reflectances) in a spatialised geometry. CrocO uses an ensemble of snowpack simulations to represent modelling uncertainties, and a Particle Filter (PF) to reduce them. The PF is known to collapse when assimilating a too large number of observations. Two variants of the PF were specifically implemented to ensure that observations information is propagated in space while tackling this issue. The *global* algorithm ingests all available observations with an iterative inflation of observation errors, while the *klocal* algorithm is a localised approach performing a selection of the observations to assimilate based on background correlation patterns. Experiments are carried out in a twin experiment setup, with synthetic observations of HS and VIS-NIR reflectances available in only a $1/6^{th}$ of the simulation domain. Results show that compared against runs without assimilation, analyses exhibit an average improvement of snow water equivalent Continuous Rank Probability Score (CRPS) of 60% when assimilating HS with a 40-member ensemble, and an average 20% CRPS improvement when assimilating reflectance with a 160-member ensemble. Significant improvements are also obtained outside the observation domain. These promising results open a way for the assimilation of real observations of reflectance, or of any snowpack observations in a spatialised context.

https://doi.org/10.5194/gmd-2020-130
Preprint. Discussion started: 10 July 2020


Geoscientific Model Development Discussions

1 Introduction

Seasonal snowpack is a key element of mountainous areas. Monitoring the evolution of its physical properties is essential to forecast avalanche hazard (Morin et al., 2020), rain-on-snow related floods (Pomeroy et al., 2016; Würzer et al., 2016) and to monitor water resources (Mankin et al., 2015). Observations alone are too scarce to monitor snowpack conditions. In-situ observations provide precise observations of several key variables, but they lack spatial representativeness and have a poor spatial coverage. Remote sensing of snowpack variables such as the height of snow (HS, (m)), snow water equivalent (SWE, $(\mathrm{kg\,m^{-2}})$), visible-near infrared (VIS-NIR) reflectance, or surface temperature, provide comprehensive information over large areas but usually have a limited temporal resolution on a small set of variables. Furthermore, these observations are usually available in fractions of simulation domains only, even for space-borne data (Davaze et al., 2018; Veyssière et al., 2019; Shaw et al., 2019). For instance, snowpack VIS-NIR reflectances from moderate resolution (250-500 m) satellites such as MODIS or Sentinel-3 can help constraining the snowpack surface properties (Dozier et al., 2009). However, in the areas covered by clouds, forests, or concerned by high sub-pixel variability (ridges, roughness, fractional snow cover) and shadows, satellite retrievals are less accurate (Masson et al., 2018; Lamare et al., in prep, 2020), and data should be filtered out (Cluzet et al., 2020).

Snowpack models of different complexity offer an exhaustive spatial and temporal coverage (Krinner et al., 2018). They are applied within several spatial configurations, including collection of points, regular or irregular grids (Morin et al., 2020). In this paper, "spatialised" refers indistinctly to any of these configurations. Only detailed snowpack models enable to assess avalanche hazard and monitor water resources alike (Morin et al., 2020), but they suffer from considerable errors and uncertainties (Essery et al., 2013; Lafaysse et al., 2017), limiting their use. In that context, combining remote sensing observations with models through data assimilation is an appealing solution (Largeron et al., submitted, 2020). It enables to optimally combine the spatial and temporal coverage of snowpack models with the available information from observations. Assimilation of optical reflectance could reduce modelled SWE errors by up to a factor of two (Charrois et al., 2016), and preliminary studies showed its potential for spatialised assimilation (Cluzet et al., 2020). Assimilation of HS is very efficient in reducing modelled SWE errors (Margulis et al., 2019). However, the limited spatial coverage of observations is stressing the need for data assimilation algorithms able to spread the snowpack observations information into the non-observed areas (Winstral et al., 2019; Cantet et al., 2019; Largeron et al., submitted, 2020).

The Particle Filter with Sequential Importance Resampling (PF, Gordon et al., 1993; Van Leeuwen, 2009) is a Bayesian ensemble data assimilation technique well suited to snowpack modelling (Magnusson et al., 2017). This sequential algorithm relies on an ensemble of model runs (particles) to represent the forecast uncertainty. At each observation date, the prior (or background) composed of the particles is evaluated against the observations. The PF posterior (or analysis) is built by replicating the particles that are nearest to the observation (with respect to the observation error) and discarding the others.
The PF could be used in a spatialised context to spread observations information as suggested by Largeron et al. (submitted,

https://doi.org/10.5194/gmd-2020-130
Preprint. Discussion started: 10 July 2020


Geoscientific Model Development Discussions

2020) and Winstral et al. (2019). This is not straightforward because of the PF degeneracy, i.e. the required number of particles scales exponentially with the number of observations (Bengtsson et al., 2008; Snyder et al., 2008). This issue is a severe drawback when considering applications of the PF on large domains with a reasonable number of particles (Stigter et al., 2017).

Several solutions exist to tackle the PF degeneracy. A first approach is to inflate the observation errors in the PF. The tolerance of the PF is increased, leading to more particles being replicated. This approach is based on the fact that observation error statistics are usually poorly known and underestimated. It can also be used as a safeguard to prevent the PF to degenerate on specific dates, when observations are not compatible with the ensemble. PF inflation was successfully implemented in point scale simulations of the snowpack (Larue et al., 2018). When dealing with a large number of observations, inflation might lead to degeneracy or null analysis (posterior equal to the prior). In this work, we generalize over space the inflation of Larue et al. (2018), trying to ingest all the observations into a single analysis over the domain, in a so-called *global* approach.

PF localisation is a more widespread alternative, tackling degeneracy by reducing the number of observations simultaneously assimilated by the PF (Poterjoy, 2016; Poterjoy and Anderson, 2016; Penny and Miyoshi, 2016; Poterjoy et al., 2019, *italic* notations are taken from the review of Farchi and Bocquet, 2018). In this method, the simulation domain is divided into *blocks* where different PF analyses are performed considering a local subset of observations (*domain*) based on a localisation radius. It makes it possible to constrain the model in locations that are not directly observed, but with nearby observations. The underlying hypothesis of localisation is that model points are independent beyond a certain distance, i.e. constraining one point with the observation from a too distant point would be meaningless, and likely degrade the analysis performance (Houtekamer and Mitchell, 1998). However, in the case of small simulation domains or modelled systems driven by large-scale coherent causalities, large scale correlations (relative to the domain size) may be physically sound, and defining a localisation radius may be a difficult task. In order to face this issue, we developed a new localisation approach called the k-localisation, where localisation *domains* are based on background correlation patterns.

These developments were implemented into CrocO (Crocus-Observations) an ensemble data assimilation system able to sequentially assimilate snowpack observations with a PF in a spatialised context. CrocO can be implemented in any geometry, (e.g. within a distributed (gridded) framework or any irregular spatial discretisation). Here, we apply CrocO in a semi-distributed framework, which is a conceptual spatialised geometry, operationally used by Météo-France for avalanche hazard forecasting (Lafaysse et al., 2013; Morin et al., 2020). This framework is similar to many topographic-based discretisation in hydrological models (e.g. Clark et al., 2015). This setup enables to account for the snowpack variability induced by the topography at the scale of a mountain range, through meteorological conditions (elevation controls the air temperature and precipitation phase) and the snowpack radiative budget (also dependent on the aspect and slope angle) (Durand et al., 1993).

CrocO uses an ensemble of stochastic perturbations of SAFRAN meteorological analysis (Durand et al., 1993; Charrois et al., 2016) to force ESCROC (Ensemble System CROCus, Lafaysse et al. (2017)), the multi-physical version of Crocus snowpack model (Vionnet et al., 2012). The ensemble setup accounts for the major sources of uncertainties in snowpack modelling (Raleigh et al., 2015) and was formerly described and evaluated in the semi-distributed geometry by Cluzet et al. (2020).

Inflation and k-localisation were implemented into CrocO. Here, we present CrocO and evaluate how it addresses the issues of reflectance observation sparseness and PF degeneracy in the context of snowpack modelling. This problem is divided into

https://doi.org/10.5194/gmd-2020-130
Preprint. Discussion started: 10 July 2020


Geoscientific Model Development Discussions

two scientific questions: (1) Is CrocO PF able to efficiently spread the information from sparse observations in space without degenerating ? (2) Is the spatial information content of reflectance valuable for snowpack models ? We assess these questions by evaluating the performance of CrocO to model the SWE when assimilating synthetic observations of HS and reflectance covering only a portion of the domain.

Section 2 presents the CrocO system, i.e. the ensemble modelling system and the PF algorithms. Section 3 introduces the evaluation methodology. Following Sec. 4 assesses the performance of CrocO and Sec. 5 discusses the results. Finally, Sec. 6 provides perspectives and research directions.

2 Material and methods

2.1 Modelling geometry

Simulations are performed in the semi-distributed geometry. Mountain ranges such as the Alps are discretized into so-called *massifs* of about 1000 km^2 to account for regional variability of meteorological conditions. Within each massif, topographic-induced variability is taken into account by running the model into a fixed set of topographic classes, e.g. by 300 m elevation bands, for 0°, 20° and 40° slopes and 8 aspects (see Fig. 1). This set enables to reproduce the main features of snowpack variability (e.g. Mary et al., 2013).

In this study, we focus on the Grandes Rousses, a single massif in the central French Alps. This area of about 500 km^2 is represented by $N_{pts} = 187$ independent topographic classes (see Fig. 1). In the following, specific topographic classes are denoted as follows: *elevation_aspect_slope*, e.g. 1800_N_40 stands for a 40° slope, with a northern aspect at 1800 m.a.s.l.

2.2 CrocO Ensemble data assimilation setup

The ensemble data assimilation workflow of CrocO is represented in Fig. 2. In the following, only a short description of the system and its elements is provided. More details on the ensemble modelling setup are available in Cluzet et al. (2020).

2.2.1 Ensemble of snowpack models

Crocus is a detailed snowpack model, enabling to represent the snowpack coupling with the ground and atmosphere in the ISBA land surface model (Interaction Soil-Biosphere-Atmosphere). It is embedded within the SURFEX_v8.1 modelling platform (SURFace Externalisée, Masson et al. (2013)). The TARTES optical scheme (Libois et al., 2013, 2015) represents VIS-NIR spectral radiative transfer within the snowpack, driven by snow metamorphism (Carmagnola et al., 2014) and Light Absorbing Particles (LAP ($\mathrm{gg}_{\mathrm{snow}}^{-1}$)) deposition fluxes (Tuzet et al., 2017). Moreover, TARTES computes the snowpack reflectance with a high spectral resolution, making the model directly comparable to the observations. This way, TARTES is both a physical component of Crocus and an observation operator.

ESCROC (Ensemble System CROCus, Lafaysse et al., 2017) multi-physical ensemble version of Crocus is used to account

https://doi.org/10.5194/gmd-2020-130
Preprint. Discussion started: 10 July 2020

Geoscientific Model Development Discussions

for snowpack modelling uncertainties. A random draw among 1944 ESCROC multi-physics configurations was performed and used in all the simulations and denoted $(M_i)_{0<i\leq N_e}$, N_e being the ensemble size (e.g. 40 or 160 members, see Fig. 2). These configurations are considered equiprobable before any data assimilation.

2.2.2 Ensemble of meteorological forcings

Meteorological forcings are taken from SAFRAN (Durand et al., 1993) reanalysis, where forecasts from the ARPEGE Numerical Weather Prediction (NWP) model are downscaled and adjusted with surface observations within the massif area. They are combined with MOCAGE LAP fluxes (Josse et al., 2004) interpolated at Col du Lautaret (2058 m.a.s.l, inside the Grandes-Rousses) to constitute the reference forcing dataset. Before the beginning of the simulation, spatially homogeneous stochastic perturbations are applied to this forcing to generate an ensemble of forcings $(F_i)_{0<i\leq N_e}$ as described in Cluzet et al. (2020). Each forcing F_i is associated with the corresponding M_i ESCROC configuration and this relation is fixed during the whole simulation.

2.2.3 The Particle Filter in CrocO

The PF is applied sequentially at each observation date on the background state vectors (soil and snowpack state variables, denoted *BG* on Fig. 2). Its analysis is an ensemble of initial conditions used to propagate the model forward. The algorithm is implemented into SODA (SURFEX Offline Data Assimilation, Albergel et al. (2017)), the data assimilation module of SURFEX_v8.1, enabling a continuous execution sequence between ensemble propagation and analysis, as depicted in Fig. 2.

2.3 The Particle Filter equations

At a given observation date, we consider a set of observed variables available at several locations, totalling N_y different observations.

- Each member $\widehat{\boldsymbol{x_b^i}}$ of the background state $\widehat{\mathbf{X_b}}$ is projected into the observation space using the observation operator h. In our case, h is just an orthogonal projection on the N_y observations since HS and reflectance are diagnosed within Crocus (see Sec. 2.2.1). The projection $\boldsymbol{x_b^i} = h\widehat{\boldsymbol{x_b^i}} = (x_k^i)_{0<k\leq N_y}$, corresponds to the modelled values at each observed variable/point.

- these N_y observations are collected in the vector $\boldsymbol{y} = (y_k)_{0<k\leq N_y}$. The associated observation error covariance matrix $\mathbf{R}$ (Eq. 1) is supposed diagonal (e.g. observation errors are assumed independent):

$$\mathbf{R} = \mathbf{diag}(\sigma_k^2, 0 < k \leq N_y) \tag{1}$$

  Where σ_k^2 stands for the observation error variance of observation k and depends only on the type of variable of observation y_k (e.g. HS or reflectance).

https://doi.org/10.5194/gmd-2020-130
Preprint. Discussion started: 10 July 2020


Geoscientific Model Development Discussions
Open Access
EGU

The PF analysis usually works in two steps.

- (1) computing the particle weights w^i as the normalised observation likelihood for each particle (Eq. 2):

$$w^i = \frac{e^{-\frac{1}{2}(\boldsymbol{y}-\boldsymbol{x_b^i})^T\mathbf{R^{-1}}(\boldsymbol{y}-\boldsymbol{x_b^i})}}{\sum_{k=1}^{N_e} e^{-\frac{1}{2}(\boldsymbol{y}-\boldsymbol{x_b^k})^T\mathbf{R^{-1}}(\boldsymbol{y}-\boldsymbol{x_b^k})}} \tag{2}$$

- (2) resampling the particles based on their weights to build the analysis vector $\widehat{\mathbf{X_a}}$. Here, we apply the PF resampling from Kitagawa (1996) which returns $\boldsymbol{s} = (s_i)_{0<i\leq N_e}$, ($s_i \in [1..N_e]$) a sorted vector with duplications, representing the particles to replicate.

A sample reordering step was added for numerical optimisation with no expected incidence on the PF behaviour (see in Appendix A2 for more details).

Two simple variants of this algorithm can be identified in a spatialised context:

- *global* approach: perform one analysis over the domain, putting all the available observations in $\boldsymbol{y}$.
- *rlocal* approach: perform one analysis per model point, assimilating only local observations, if any. This corresponds to a localised PF with *block* and *domain* size of 1.

2.3.1 Particle Filter degeneracy

Degeneracy occurs when only a small fraction of the particles have non-negligible weights, resulting in a sample $\boldsymbol{s}$ where only a few different indices are present. It can be diagnosed from the weights using the effective sample size N_{eff} (Liu and Chen, 1995; Doucet et al., 2001):

$$N_{\text{eff}} = \frac{1}{\sum_{i=1}^{N_e}(w^i)^2} \tag{3}$$

With a degenerate sample, $N_{\text{eff}} \gtrsim 1$, and with innocuous analysis (all particles are replicated) $N_{\text{eff}} = N_e$.

A first approach to mitigate degeneracy is to use inflation. This method iteratively inflates $\mathbf{R}$ values until the sample population is large enough. Here, we develop a variant from Larue et al. (2018) method, which was not explicitly relying on N_{eff} (Eq. 3) . Consider applying an inflation factor $\frac{1}{\alpha}$ to $\mathbf{R}$, ($0 < \alpha \leq 1$, $\alpha = 1$ being the value for no inflation), and update N_{eff} (Eqs. 2 and 3): N_{eff} is naturally a decreasing function of α (the more we inflate $\mathbf{R}$ the more different particles will be replicated). The idea of our method is to ensure that N_{eff} exceeds a target value, N^*_{eff}. If $N_{\text{eff}} < N^*_{\text{eff}}$ (degenerate case), we reduce α (inflate) until $N_{\text{eff}} = N^*_{\text{eff}}$ using Alg. 1. In the following, inflation is used in the *global* and *rlocal* PF (see Sec. 2.2.3).

The core of Alg. 1 is an hybrid bisection-secant method to find the zero of $f : \alpha \mapsto N_{\text{eff}}(\alpha) - N^*_{\text{eff}}$ in $[0, 1]$. It is inspired on **rtsafe** algorithm (Vetterling et al., 1992). The **guess** function computes a new guess α_2 to minimize f. Note that in the unlikely case where Alg. 1 does not converge, all the particles are replicated.

https://doi.org/10.5194/gmd-2020-130
Preprint. Discussion started: 10 July 2020

Geoscientific Model Development Discussions
Open Access
EGU

Algorithm 1 Weighting algorithm with inflation.

Input: $\boldsymbol{x^i}, \boldsymbol{y}, \mathbf{R}, N^*_{\text{eff}}$

Output: $\boldsymbol{w^i}$

$\alpha \leftarrow 1$
$\mathbf{R} \leftarrow \frac{1}{\alpha}\mathbf{R}$
$\boldsymbol{w^i} \leftarrow$**weights(**$\boldsymbol{x^i}, \boldsymbol{y}, \mathbf{R}$**)** (Eq. 2)
$N_{\text{eff}} \leftarrow$**eff_weights(**$w^i$**)** (Eq. 3)
if $N_{\text{eff}} < N^*_{\text{eff}}$ **then**
  $\alpha_1 \leftarrow 0$
  $N_{\text{eff}_1} \leftarrow N_e$
  $cond \leftarrow True$
  $i \leftarrow 0$
  while $cond$ **do**
    $\alpha_2 \leftarrow$**guess(**$\alpha_1, \alpha, N_{\text{eff}_1}, N_{\text{eff}}, N^*_{\text{eff}}$**)**
    $\mathbf{R} \leftarrow \frac{1}{\alpha_2}\mathbf{R}$
    $w_2^i \leftarrow$**weights(**$\boldsymbol{x^i}, \boldsymbol{y}, \mathbf{R}$**)** (Eq. 2)
    $N_{\text{eff}_2} \leftarrow$**eff_weights(**$w_2^i$**)** (Eq. 3)
    if $|N_{\text{eff}_2} - N^*_{\text{eff}}| < \epsilon$ **then**
      $cond \leftarrow False$
      $\alpha \leftarrow \alpha_2$
      $w^i \leftarrow w_2^i$
    else
      $\alpha \leftarrow \alpha_1$
      $\alpha_1 \leftarrow \alpha_2$
      $N_{\text{eff}} \leftarrow N_{\text{eff}_1}$
      $N_{\text{eff}_1} \leftarrow N_{\text{eff}_2}$
    end if
    $i \leftarrow i + 1$
    if $i = maxiter$ **then**
      print "failed to converge, duplicating all particles"
      $w^i \leftarrow \frac{1}{N_e}$
    end if
  end while
end if

https://doi.org/10.5194/gmd-2020-130
Preprint. Discussion started: 10 July 2020


Geoscientific Model Development Discussions

2.3.2 k-localisation

In the k-localisation algorithm, degeneracy is mitigated by reducing the number of observations simultaneously assimilated. The PF analysis is applied to each simulation point sequentially. In order to build the analysis at point n, background correlations $\mathbf{B}_{\boldsymbol{v}}$ are computed for each variable v (e.g HS or reflectance) between n and all the observed points. In a first step, all observations from points exhibiting significant background correlations (see below **select_k_biggest** function) are used. If the PF degenerates, the number of observations is progressively decreased until degeneracy is mitigated. As earlier, degeneracy is considered mitigated when $N_{\text{eff}} \geq N^*_{\text{eff}}$. This way, we ensure that a maximal number of observations has been ingested by the PF without degenerating.

In case of degeneracy, the observation point displaying the lowest correlation is ruled out. The PF weights are computed (Eq. 2), and a new effective sample size is derived (Eq. 3). While the target sample size is not exceeded, this selection proceeds iteratively. The notation k in "k-localisation" refers to the number k of retained observations of each variable. This approach is similar to EnKF localisation algorithm where the localisation *domain* is based on background correlations (Hamill et al., 2001).

The detailed k-localisation algorithm is described in Alg. 2, where:

- The **select_k_biggest** method returns for each variable, the domain $\boldsymbol{d_v}$, of up to k observed points (named p) that are the most correlated (in absolute value) with n, and match the following criteria:
  - in $\widehat{\boldsymbol{x_v^i}}$, there are at least 10% of members defined in both points (reflectance is not defined when there is no snow)
  - $|\mathbf{B}_{\boldsymbol{v}}(n,p)| > 0.3$: correlations are significant.
- $\boldsymbol{d}$ is the collection of the domains $\boldsymbol{d_v}$
- **extract_points** extracts $\boldsymbol{d}$ from $\boldsymbol{y}, \boldsymbol{x^i}$ and $\mathbf{R}$.

2.3.3 Particle Filter and reflectance observations

Assimilating reflectance with the PF requires some adaptations. Snow reflectance is a bounded variable (0-1) and is not defined in the absence of snow. For this reason, reflectances of snow-free members and observations were set to 0.2 (snow-free ground reflectance value in Crocus) in the PF Eq. 2 (Sec. 2.2.3).

3 Evaluation strategy

Our strategy is to assess the performance of the analysis by means of twin experiments, i.e. using synthetic observations. The assimilation run is compared to an identical run without assimilation (openloop run). Synthetic observations are extracted from a model run and assimilated. These observations allow to mimic real observations with a perfect knowledge of the true state. Analysis and openloop experiments can therefore be compared with this true state anywhere, for any variable. It allows in a

https://doi.org/10.5194/gmd-2020-130
Preprint. Discussion started: 10 July 2020

Geoscientific Model Development Discussions

Algorithm 2 k-localisation algorithm

Input: $\boldsymbol{x^i}$, $\boldsymbol{y}$, $\mathbf{B}$, $\mathbf{R}$, N^*_{eff}
Output: $(\boldsymbol{w_n^i})_{0<n\leq N_e}$

for $n = 1$ to N_{pts} **do**
  $k \leftarrow k_{max}$ {try to ingest all available observations.}
  $cond \leftarrow True$
  while $cond$ **and** $k > 0$ **do**
    for $v = 1$ to N_v **do**
      $\boldsymbol{d_v} \leftarrow$ **select_k_biggest(**n,k,$\mathbf{B_v}$,$\boldsymbol{x_v^i}$, $\boldsymbol{y}$**)**
    end for
    $\boldsymbol{y_k}, \boldsymbol{x_k^i}, \mathbf{R_k} \leftarrow$ **extract_points(**$\boldsymbol{y}$, $\boldsymbol{x^i}$,$\mathbf{R}$, $\boldsymbol{d}$**)**
    $w_n^i \leftarrow$ **weights(**$\boldsymbol{x_k^i}, \boldsymbol{y_k}, \mathbf{R_k}$**)** (Eq. 2)
    $N_{\text{eff}} \leftarrow$ **eff_weights(**w_n^i**)** (Eq. 3)
    if $N_{\text{eff}} \geq N^*_{\text{eff}}$ **then**
      $cond \leftarrow False$
    end if
    $k \leftarrow k - 1$
  end while
  if $k = 1$ **then**
    $w_n^i \leftarrow$ **inflation(**$\boldsymbol{x_k^i}$,$\boldsymbol{y_k}$,R_k, N^*_{eff}**)**
  end if
end for

first step to get rid of the error and bias issues inherent to real observations (Cluzet et al., 2020), a reason why we did not add any noise to the synthetic observations as commonly done in twin experiments (Lahoz and Menard, 2010). This way, we can focus on the two following questions (see Sec. 1):

- Is CrocO PF able to efficiently spread the information from sparse observations into space without degenerating ?
- Is spatial information content of reflectance a valuable source of information for snowpack models ?

In order to disentangle these questions, we run baseline experiments assimilating synthetic observations of HS which is strongly linked with SWE (Margulis et al., 2019). These experiments are used to evaluate the PF algorithms efficiency, and as a baseline for synthetic reflectance assimilation experiments evaluating the information content of reflectance.
Three different algorithms are evaluated: the *global* algorithm (with inflation), the *rlocal* algorithm (with inflation) and the k-localized algorithm *klocal*.

https://doi.org/10.5194/gmd-2020-130
Preprint. Discussion started: 10 July 2020


Geoscientific Model Development Discussions

3.1 Experiments

3.1.1 Twin experiments setup

In our twin experiment setup, an openloop ensemble is used as a reference and to generate synthetic observations. Openloop simulations are carried out with CrocO for 4 consecutive winters (2013-2017) in the Grandes-Rousses (see Sec. 2.1), with 160 members. For each year, the integral of SWE over time and space is computed from each member, and members corresponding to the 20th, 40th, 60th and 80th percentiles of the ensemble are extracted to be used as synthetic observations (denoted *year_ppercentile* e.g. 2014_p80). Before any assimilation experiment, the openloop member ($F_i - M_i$ couple in Fig. 2) used as true state is withdrawn and replaced by a new random member.

The spatial coverage of synthetic observations was reduced, mimicking a typical reflectance mask. Synthetic observations were only available above an assumed constant tree line at 1800 m (see Fig. 1), and not available in steep slopes (over 20^o) and in northern aspects (shadows, considering a daily satellite pass around 10-11:00 UTC.), for the whole snow season. As a result, in this case, only 35 (over 187) topographic classes are observed. Observation date were chosen corresponding to clear-sky days with a MODIS overpass, resulting in an approximately weekly frequency (e.g. Revuelto et al. (2018); Cluzet et al. (2020)).

Considering reflectance, a minimal set of two different bands is used, corresponding to MODIS sensor band 4 (555 nm) and 5 (1240 nm) (Charrois et al., 2016). Observation error variances is set to $1.0 \times 10^{-2}\mathrm{m}^2$ for HS and 5.6×10^{-4} and 2.0×10^{-3} for band 4 and band 5 reflectance respectively (Wright et al., 2014). These values are only initial values for the inflation in the *global* and *rlocal* algorithms. Since the *klocal* algorithm uses only inflation if k drops to 1 (see Sec. 2), observation error variances are multiplied by a factor of 5 to enable the *klocal* algorithm to ingest observations from several points.

In order to study the ability of the *global*, *klocal* and *rlocal* algorithms to spread the information in space, a first set of experiments is conducted assimilating HS with 40 members (see setup in Tab. 1). In order to evaluate the algorithms ability to assimilate reflectance (Band 4 and Band 5) a second set of experiments is conducted, other things being equal (Tab. 2). The ensemble size is increased from 40 to 160 in a third set of experiments assimilating reflectance, in order to analyse the influence of a larger ensemble on the algorithms performance (Tab. 3). Note in Tab. 1-3 that N^*_{eff} is adjusted to the ensemble size, in order to preserve $N_e/N^*_{\mathrm{eff}} \approx 5-7$ following Larue et al. (2018).

3.2 Evaluation Scores

The performance of the assimilation and openloop run is evaluated against the synthetic truth using several scores. The Absolute Error of the ensemble mean (AE) and ensemble spread σ are two common metrics of ensemble modelling. Given an ensemble $E_{m,c,t}$ of N_e members m in topographic class c at time t and the corresponding observations $o_{c,t}$, the ensemble mean is described by Eq. 4:

$$\overline{E}_{c,t} = \frac{1}{N_e} \sum_{m=1}^{N_e} E_{m,c,t} \tag{4}$$

https://doi.org/10.5194/gmd-2020-130
Preprint. Discussion started: 10 July 2020


Geoscientific Model Development Discussions

From which we can compute the absolute error AE (Eq. 5) and the spread (or dispersion) σ (Eq. 6):

$$AE_{c,t} = |\overline{E}_{c,t} - o_{c,t}| \quad \forall (c,t) \in [1, N_{pts}] \times [1, N_t] \tag{5}$$

$$\sigma_{c,t} = \sqrt{\frac{1}{N_e} \sum_{m=1}^{N_e} (E_{m,c,t} - \overline{E}_{c,t})^2} \quad \forall (c,t) \in [1, N_{pts}] \times [1, N_t] \tag{6}$$

Where N_t is the number of evaluation time steps.

The Continuous Ranked Probability Score (CRPS, (Eq. 7) Matheson and Winkler, 1976) evaluates the reliability and resolution of an ensemble based on a verification dataset. An ensemble is reliable when events are forecast with the right probability, and has a good resolution when it is able to discriminate distinct observed events. For a reliable system, the resolution is equivalent to the sharpness, which is the spread of the produced forecasts.

If we denote $F_{c,t}$ the Cumulative Distribution Function (CDF) and $O_{c,t}$ the corresponding observation CDF (Heaviside function centred on the truth value), the CRPS is computed at (c,t) following:

$$\text{CRPS}_{c,t} = \int_{\mathbb{R}} (F_{c,t}(x) - O_{c,t}(x))^2 dx \quad \forall (c,t) \in [1, N_{pts}] \times [1, N_t] \tag{7}$$

In this work, $\text{CRPS}_{c,t}$ value is averaged over time alone or time and space depending on the desired level of aggregation.
The CRPS can be decomposed in two terms following Hersbach (2000) (Eq. 8):

$$\text{CRPS} = \text{Reli} + \text{Resol} \tag{8}$$

Where Reli quantifies the reliability of the ensemble. The associated skill scores (CRPSS and ReliS) can be used to compare the performance of an ensemble E to a reference R, here, the openloop run:

$$\text{CRPSS}(E) = 1 - \frac{\text{CRPS}(E)}{\text{CRPS}(R)} \tag{9}$$

A skill score of 1 denotes a perfect score, 0 a neutral performance and $-\infty$ is the worst achievable skill score.

4 Results

4.1 Preliminary Results

4.1.1 Impact of the inflation

The inflation algorithm was introduced by Larue et al. (2018) in point scale simulations but to the best of our knowledge, never applied in a spatialised context. Here we evaluate its impact on the *global* algorithm by switching it on/off. As an example, Fig. 3 shows the impact of the inflation on SWE when assimilating the HS of 2015_p80 (as defined in Sec. 3.1.1) member with

https://doi.org/10.5194/gmd-2020-130
Preprint. Discussion started: 10 July 2020


Geoscientific Model Development Discussions

the *global* algorithm, in a topographic class which is not observed (1800_N_40, as defined in Sec. 2.1). This choice of member and topographic class is well representative of the impact of the inflation on the *global* algorithm.

In this case, both inflation ($N^*_{\text{eff}} = 7$) and no inflation ($N^*_{\text{eff}} = 1$) lead to a significant reduction of the ensemble spread compared with the openloop (Fig 3a-b). From January 2015 until the peak of SWE in mid-April 2015, (Fig. 1c) the simulation with inflation has significantly lower errors than without inflation and the openloop (10-20 $\mathrm{kg\,m^{-2}}$ vs. 60-80 $\mathrm{kg\,m^{-2}}$ and 30-50 $\mathrm{kg\,m^{-2}}$ respectively), leading to a better agreement with the synthetic truth in the melting season (Fig. 3a). During the melting season (mid-April 2015 onwards), the RMSE of the assimilation algorithms is reaching a peak, coinciding with an absence of observations. In comparison, the openloop RMSE is smaller in the first part of the melting season, but the spread is three times larger, making it almost uninformative. For several analyses (2014, November 21$^{\text{th}}$, and 2014, December 30th for example) the ensemble spread without inflation drops to 0 while its RMSE strongly increases compared to the openloop, suggesting that it is prone to degeneracy.

4.1.2 Correlation patterns

The *klocal* algorithm relies on background correlation patterns to define localisation *domains*. To illustrate the potential of using such information in the PF, Fig. 4 shows the correlation patterns of the 40 members openloop in a non observed topographic class (1800_N_40, red dot) in the mid-winter, several months after the snow season onset (2015, February 20$^{\text{th}}$) for the different assimilation variables. These variables exhibit strong but contrasted correlation patterns. Band 4 (Fig. 4a) correlations are generally high (0.6-1) and uniform. Many of the observed classes (black dots) are strongly correlated with the considered class as for HS (Fig. 4c). Band 5 (Fig. 4b) exhibits significant correlations, in particular across slopes. However, they are more restricted to the northern aspects, only a few observed classes in the Eastern aspects being significantly correlated with the considered class. Finally, note that these patterns vary with time but remain significant along the whole season (not shown), and that increasing the ensemble size up to 160 leads to identical patterns (not shown).

4.2 Results of the experiments

4.2.1 Assimilation of Snow Depth

In a first step, assimilation of HS from the different synthetic members was launched to serve as a reference for reflectance assimilation. Fig. 5 shows the CRPSS (Eq. 9, aggregated over time only) of the HS assimilation with the three PF algorithms considering the synthetic member 2013_q20 as reference. Results for this specific synthetic member were chosen here as a representative example of the algorithms performance.

The *rlocal* performance compared with the openloop is high (0.7-1), but limited to the observed classes (black dots) since there is no spatial propagation in this algorithm. *global* and *klocal* algorithms have similar, overall good performance, managing to strongly reduce modelling uncertainties except at very low altitudes (600-900 m), (skills of -0.2) where snow does not usually

https://doi.org/10.5194/gmd-2020-130
Preprint. Discussion started: 10 July 2020


Geoscientific Model Development Discussions

last for more than a few weeks.

This behaviour may vary with the snow conditions, i.e., between the different assimilated synthetic members and from one year to another. In order to generalize this result, Fig. 6 shows the CRPS and Reli (aggregated over time and space) of the different algorithms for the 16 synthetic members and differentiated between observed and non-observed classes. CRPS and Reliability are considerably reduced compared with the openloop (by a factor of 2-3 and 4-5, respectively) for all the algorithms in the observed classes. This suggests that the PF manages to reduce the spread of the ensemble while reducing its errors. In the non observed classes, the gain is almost as good (CRPSS of 0.6) except for the *rlocal* algorithm, which is identical to the openloop as expected. No significant difference of skill is obtained between *global* and *klocal* algorithms.

4.2.2 Assimilation of Reflectance

Optical reflectance is a promising assimilation variable due to its extended availability in satellite observations, but assimilation of reflectance is not expected to constrain bulk variables like SWE or HS as well as HS assimilation. Here, we conduct reflectance assimilation in the same setup as in Sec 4.2.1, all other things equal, to assess this difference.

Fig. 7 shows the performance of the reflectance assimilation for the 16 synthetic members with 40 members (filled boxes). The different algorithms only lead to moderate improvements in CRPS (median CRPSS of 0.-0.2, median ReliS of 0.2-0.4). Moreover, the *global* and *klocal* algorithms frequently degrade the performance, suggesting that this configuration is not robust.

Suspecting that 40 members is insufficient to well represent the multivariate probability density function of reflectance and other model variables, the ensemble size was increased to 160 (hatched boxes), leading to significant improvements in the performance and robustness of the algorithms (median CRPSS of 0.2, median Reli of 0.4-0.6). Reliability of the *global* algorithm is significantly improved with respect to the *klocal* algorithm.

Fig. 8 shows the spatial performance of the different algorithms for member 2016_p60. Spatial patterns similar to the HS assim are found. *rlocal* performance is limited to the observed classes, while *global* and *klocal* manage to improve the simulations across aspects and slopes. However, Skill scores are lower than for HS (0.2-0.5), and the performance of all algorithms is poor at lower elevations, even in some of the observed classes.

5 Discussion

In this section, we discuss the performance of CrocO PF algorithms using the assimilation of HS, and consider the potential of the assimilation of reflectance in view of assimilating real data.

5.1 Tackling Particle Filter degeneracy

Because they assimilate several observations at the same time, *global* and *klocal* approaches could be prone to PF degeneracy. However, they almost never degrade the performances when assimilating HS in a variety of years and synthetic members

https://doi.org/10.5194/gmd-2020-130
Preprint. Discussion started: 10 July 2020


Geoscientific Model Development Discussions

percentiles (Fig. 6). This suggests that either inflating the observation errors (as demonstrated by Larue et al. (2018), a result we have generalized in space) or exploiting background correlations to reduce the number of assimilated observations, are two efficient approaches to tackle degeneracy.

In several cases though, a strong degradation of score occurs when assimilating reflectance (Fig. 7), which could either be attributed to an algorithmic failure in the PF, or an intrinsic lack of informativeness of reflectance in some situations. Based on the good behaviour of the algorithm with HS, and because by construction, *global* and *klocal* algorithms cannot lead to a degenerate PF sample we consider this comes from the reflectance itself (this point will be further discussed in the following sections).

Beyond tackling degeneracy, *global* and *klocal* algorithms also beat the *rlocal* approach on Reli and CRPS scores (Figs. 7 and 8). This suggests that assimilating multiple observations increases the quality of the PF analysis, even locally. More precisely, most of the improvement is due to the Reli term of the CRPS. This property is key for ensemble modelling, because it ensures that events are forecasted with a right probability. However, this is not sufficient, e.g. the climatology has a perfect reliability but is not informative at all. Successful assimilation manages to improve general metrics such as the CRPS while improving the reliability. On this aspect, the *global* and *klocal* algorithms have a satisfying performance.

5.2 Propagating the observations information

Having sparse observations is one of the most challenging tasks for data assimilation systems of snowpack observations (Magnusson et al., 2014; Largeron et al., submitted, 2020). In our partially observed, conceptual setup, the *global* and *klocal* PF variants developed here efficiently propagate the observations information to the non-observed classes, with generally a better performance than the openloop and the *rlocal* approach in the non-observed classes when assimilating HS (Fig. 5). The algorithms performance is particularly good across aspects and slopes with only a few steep, northern aspect slopes exhibiting neutral to poor performances (Figs. 5 and 8). This suggests that southern aspect and flat classes are informative on the majority of the simulation domain. Conversely, considering that there are strong background correlations between the western and eastern sides of the domain, we can speculate that observing either side could yield overall good results.

On these figures, propagation of the information is limited towards lower elevation (600-1200 m). At such elevation, the snow cover is usually intermittent and a good discrimination of the precipitation phase is crucial. The PF does this indirectly through HS and reflectance observations, because rain causes a decrease of HS through compaction and melting while reflectance also decreases because of because of quick isothermal metamorphism. However, in our setup, the lowest observed elevation is 1800 m, therefore indirect observation of the rain-snow line positioning under this level is not possible, potentially explaining the moderate performance of the PF there. In that case, assimilation of Snow Cover Fraction might be the best solution: since the snowpack is intermittent there, the informativeness of this variable is maximal (Aalstad et al., 2018).

Global and *klocal* algorithms exhibit strong performances when assimilating HS (Fig. 5), and moderate performances for reflectance. HS is well linked with the SWE (by the bulk density) and the interest of this variable for data assimilation is clear

https://doi.org/10.5194/gmd-2020-130
Preprint. Discussion started: 10 July 2020

(Margulis et al., 2019). Though the performance is lower for Reflectance, it remains considerable and in line with previous results on point simulations (Charrois et al., 2016), with an average score improvement of 20-40%.

An outstanding result here, is that our study suggests that reflectance information can be spread from southern slopes to the northern ones, although in many situations, the snowpack evolves in different ways between these aspects. For example, in sunny conditions, melt and wet metamorphism will cause a drop in reflectance in southern slopes, while reflectance will not evolve much in northern slopes. Therefore, a reflectance observation in a southern slope is not necessarily informative on reflectance value in the northern aspect per se. It is informative however, in our ensemble data assimilation framework. Indirectly, in this case this observation could enable the PF to reject all the ensemble members that did not have an appropriate meteorological forcing (snowfall or cloud cover would lead to wrong reflectance values), or multiphysical parametrisations, thus enabling to correct the ensemble in the whole domain. These insights are consistent with the study of Winstral et al. (2019), where in situ observations are used to correct meteorological forcing parameters across large simulation domains.

5.3 Towards the assimilation of real observations of reflectance

Reflectance is an appealing variable for snowpack modelling because of its sensitivity to snowpack surface properties (Dozier et al., 2009) and the abundance of moderate-resolution space-borne sensors (MODIS, Sentinel2-3, VIIRS, Landsat...) providing us with a handful of observations to assimilate, contrary to HS. This study demonstrates the potential of the PF to spread information and assimilate reflectance with a positive impact (Sec. 5.2). Yet, assimilating real observations is another challenge, for two reasons.

First, space-borne reflectance observations are usually noisy and biased (e.g. Cluzet et al., 2020). Satellite retrievals could be improved in the future (Kokhanovsky et al., 2019; Lamare et al., in prep, 2020), and Cluzet et al. (2020) showed that assimilating ratios of reflectance could be a workaround to tackle this issue. However, the required accuracy for reflectance retrieval to remain informative on the snowpack properties is high (Warren, 2013), and it is yet to prove whether either approach can achieve this requirement.

Second, in this twin experiment framework, spatial patterns of the synthetic observations are likely compatible with the ensemble since they come from the same modelling system. This may not be the case in reality, therefore making it more difficult to assimilate, and we refer to this issue as model or ensemble realism.

We must assess the strengths and weaknesses of the *global* and *klocal* approaches facing those two issues. The *global* algorithm assumes that a global optimum can be found across the whole domain, e.g. the information from the different observations is consistent and can be ingested in one block by the PF. With this strategy, the degeneracy due to the size of the observation vector is efficiently mitigated by the inflation algorithm as discussed in Sec. 5.1. The *klocal* approach considers that only a fraction of the observation information is relevant to constrain the model state at a given location. This algorithm tries to ingest as much information as possible while rejecting observations coming from too statistically different snowpack conditions. As a consequence, because we do not account for the real spatial patterns of observation errors, and because we work in a twin experiment setup, a global optimum on the whole domain can exist and can be found by the *global* algorithm. This might be

https://doi.org/10.5194/gmd-2020-130
Preprint. Discussion started: 10 July 2020


Geoscientific Model Development Discussions

a reason why it beats the *klocal* approach (Figs. 6 and 7). In the real world, from the model point of view, there might be contradictory informations among the observations that would be difficult to disentangle with a *global* strategy. The *klocal* algorithm could be more suited to this situation, because it is looking for local optima, based on the assumption that background correlation patterns are realistic.

These background correlation structures could be overestimated by the ensemble, and tests with real observations are necessary. Strong Band 4 correlations might be due to the spatially homogeneous perturbations of LAP fluxes used to force the simulations (see Sec. 2.2.2), a key driver of this variable. Several studies suggest that LAP fluxes vary with elevation and other topographic parameters (de Magalhães et al., 2019; Sabatier et al., 2020), but to date no reliable model for that exists in complex terrain. In such a context, assuming uniform LAP forcing seems a reasonable compromise. Strong and almost uniform correlations in HS might be caused by the spatial homogeneity of precipitation perturbations and because we do not account for snow transport by the wind and gravitational redistribution of snow (Wayand et al., 2018). Despite this semi-distributed framework suffers from obvious limitations, NWP models still suffer for large errors in mountainous areas, hampering the potential for high-resolution snowpack modelling (Vionnet et al., 2016; Fiddes et al., 2019).

In the future, improving the realism of ensemble correlations could make the spreading of information an even more challenging task with the *klocal* algorithm. But there should remain significant potential for information propagation, as results at a larger scale suggest (Magnusson et al., 2014; Cantet et al., 2019). The potential de-correlation of topographic classes would also impact the *global* algorithm. In a non-observed class, constraining the state of the snowpack with information from area that are not linked with it would likely degrade the forecasting skill, as suggested by the poor performance of the algorithms at low altitudes (Figs. 5 and 8). On the contrary, applying CrocO into larger domains (e.g. distributed simulations or a collection of semi-distributed *massifs*), would probably see the *klocal* algorithm take the best over the *global*. The increased domain size would make it less plausible to find a global optimum over the domain, whereas spatial flexibility would be an asset of the *klocal* algorithm.

5.4 Outlook for ensemble modelling and data assimilation

In the snowpack modelling community, ensemble modelling appears as a powerful tool to represent modelling uncertainties (Vernay et al., 2015; Richter et al., 2020) and for data assimilation (Essery et al., 2013; Lafaysse et al., 2017; Piazzi et al., 2018; Aalstad et al., 2018). This study offers a novel approach to extract valuable information on the snowpack spatial behaviour from spatial correlation patterns of the ensemble. These patterns could be used to diagnose links between locations, transfer information between areas, or assess the representativeness of point simulations. More broadly, ensemble background correlations have been exploited for long in the NWP and oceanographic communities to refine modelling errors representation which led to significant improvements in the DA systems (Evensen, 2003; Buehner, 2005).

Ensembles might open a way for the assimilation of point scale observations, or sparse remotely-sensed observations into spatialised simulations of the snowpack as suggested by Winstral et al. (2019) and the present work. For instance, there are

https://doi.org/10.5194/gmd-2020-130
Preprint. Discussion started: 10 July 2020


Geoscientific Model Development Discussions

numerous snow gauges and snow pit observations in the ski resorts of the French Alps. These data could be assimilated to correct the ensemble in spatialised simulations (Winstral et al., 2019). The spatial pattern of assimilated observations in the experiments of Sec. 4 do not correspond to the real-life spatial coverage of this kind of observations. To give an insight of their potential, we also applied our methodology to assimilate only five synthetic HS observations with the *global* PF in the 1200 m to 2400 m flat classes. The results are shown in Fig. 9. The assimilation improves the performance in all aspects and slopes. Naturally, this suffers from the same limitation as discussed in Sec. 5.3, not to mention the limited spatial representativeness of in situ observations but it shows some potential for this idea.

In that way, a more rational use of the available observations could be implemented towards a new ensemble data assimilation system. In the present CrocO system, SAFRAN reanalysis are only assimilating weather station information (precipitation phase, temperature, wind), and makes no use of the numerous snow observations available. Here, snow observations are assimilated by the PF, but are not used to correct meteorological forcings (only snow variables, see Fig. 2). In the way of a new ensemble data assimilation system, within CrocO, the SAFRAN meteorological analysis could be bypassed, the PF operating directly both on the meteorological and snowpack variables in a more comprehensive and coupled strategy.

6 Conclusions

In this study, we introduced CrocO, a new ensemble data assimilation system able to reduce the errors of a spatialised snowpack model in locations that are not observed. The ensemble is built by a combination of meteorological and multi-physical ensembles to represent modelling uncertainties. A Particle Filter assimilates observations of HS and Reflectance. We developed two variants of the PF using inflation or k-localisation, in order to spread the information from partial observations of the system, without degeneracy of the PF. We have shown in particular that:

1. these variants are able to ingest numerous observations without degeneracy;
2. an efficient spreading of the observations information towards the non observed areas is achieved with the *global* and *klocal* approaches;
3. reflectance assimilation leads to an overall 20% improvement in CRPS and 60% in reliability.

We suggest that this approach could be used in any spatialised framework to assimilate sparse observations from e.g. networks of in-situ snowpack observations. Beyond the snowpack modelling community, the inflation and k-localisation strategies could help address the problem of partially observed systems. This work is also a first step towards the operational assimilation of reflectance in a semi-distributed context. To reach that goal, biases of reflectance retrievals should be studied, and observation errors structures duly quantified. Snow Cover Fraction would be a good companion variable to assimilate at lower elevations, requiring the use of an appropriate observation operator. Extending the simulation domain to several massifs would allow the exchange of information between neighbouring massifs with the *klocal* algorithm.

https://doi.org/10.5194/gmd-2020-130
Preprint. Discussion started: 10 July 2020


Geoscientific Model Development Discussions

Code availability. The Crocus snowpack model (including all physical options of the ESCROC system) and the Particle Filter algorithm are developed inside the opensource SURFEX project. The source files of SURFEX code are provided at https://doi.org/10.5281/zenodo.3774861 to guarantee the permanent reproductibility of results. However, we recommend potential future users and developers to access to the code from its git repository (git.umr-cnrm.fr/git/Surfex_Git2.git) to benefit from all tools of code management (history management, bug fixes, documentation, interface for technical support, etc.). This needs a quick registration, the procedure is described at https://opensource.cnrm-game-meteo.fr/projects/snowtools/wiki/Procedure_for_new_users. The version used in this work is tagged as CrocO_v1.0.

A python software called CrocO_toolbox was specifically developed, in order to pre-post process and launch CrocO experiments. It is available on Github (https://github.com/bertrandcz/CrocO, release v1.0) along with a documentation.
The article version of CrocO_toolbox is archived at: https://doi.org/10.5281/zenodo.3784980. This software strongly relies on two external python projects ensuring the files management between the different steps of a simulation and the interface with Meteo-France HPC system (including parallelization and data storage): snowtools and vortex. Their sources are available at https://doi.org/10.5281/zenodo.3774861 (same archive as SURFEX) to guarantee the permanent reproducibility of results. However, as for the SURFEX project and for the same reasons, it is recommended to access snowtools code from its git repository (git.umr-cnrm.fr/git/snowtools_git.git). The version used in this work is also tagged as CrocO_v1.0. The vortex project gathers all environment-specific codes of Météo-France modelling systems relative to its HPC computing system. For this project, only the sources which are specific to this article simulations are provided. The common objects inheritance is based on Vortex version 1.6.1. The version used in this work is also tagged as CrocO_v1.0 in the vortex git repository.

Because these softwares could not be applied outside Météo-France HPC environment, CrocO python software offers the possibility to run CrocO simulations locally. This functionality was not used here due to the high numerical cost of our simulations, which required the use of Météo-France HPC environment.

Data availability. Input and output data necessary to reproduce the manuscript simulations and figures are provided at https://doi.org/10.5281/zenodo.3775007. This archive includes : SAFRAN reanalyses, (also available at https://doi.org/10.25326/37), MOCAGE forcings, namelists, configuration files and spinup files enabling to reproduce the simulations. Raw model outputs can be provided on request but since they amount up to 500+ Gigabytes, only post-processed simulations outputs are provided in this archive, along with scores and scripts to reproduce the manuscript figures.

Appendix A: Complements on the implementation

A1 Technical implementation and code performance

CrocO is implemented within Météo-France HPC (High Performance Computing) environment, enabling to fully parallelize the ensemble (one core per member), and bridge the gap with operational applications (Lafaysse et al., 2013; Morin et al., 2020). This implementation is strongly parallel. As an example, the execution time of a one-year assimilation run of 187 model points with 160 members on 4 nodes of 40 cores each lasts for only two hours. The PF is a lightweight algorithm, most of the computational burden owing to the propagation of the ensemble. Note also that no significant difference in execution time can

https://doi.org/10.5194/gmd-2020-130
Preprint. Discussion started: 10 July 2020


Geoscientific Model Development Discussions

505 be noted between the different PF algorithms.

A2 PF sample reordering

As mentioned in Sec. 2.3, a reordering step was implemented after the PF resampling from Kitagawa (1996), for practical reasons.

- (3) from $\boldsymbol{s}$, build $\tilde{\mathbf{s}}$ such that all elements of the unique values of $\boldsymbol{s}$ lie in the position given by their value. Example with 16 particles:

$$\boldsymbol{s} = [1,1,2,3,3,3,8,8,9,9,9,9,9,16,16,16] \Rightarrow \tilde{\mathbf{s}} = [1,2,3,1,3,3,8,8,9,9,9,9,9,16,16,16]$$

510 Indeed, I/O represents a bottleneck in the PF. When building the analysis $\widehat{\mathbf{X}^{\mathbf{a}}}$, the background $\widehat{\mathbf{X}^{\mathbf{b}}}$ is already loaded in memory. Since $\widehat{\mathbf{X}^{\mathbf{a}}}$ is just a reordering of $\widehat{\mathbf{X}^{\mathbf{b}}}$ columns based on $\boldsymbol{s}$, a reordering of $\boldsymbol{s}$ avoids to build a copy of $\widehat{\mathbf{X}^{\mathbf{b}}}$. This way, $\widehat{\mathbf{X}^{\mathbf{a}}}$ is built by an online modification of $\widehat{\mathbf{X}^{\mathbf{b}}}$ using two pointers. Reordering is a growing consideration in the PF community (Farchi and Bocquet, 2018).

Author contributions. BC wrote the manuscript, BC, ML and MD designed the study, BC developed the code with help from ML, L-FM and
515 CA. BC, MD, ML and EC designed the PF variants. All authors contributed to results analysis and discussion.

Competing interests. The authors have no competing interests to declare.

Acknowledgements. The authors are grateful to François Tuzet, Jesus Revuelto, Rafife Nheili, César Deschamps-Berger, Stéphanie Faroux (SODA) and Matthieu Vernay for their precious help in collecting input data and code implementation. They also would like to thank Fanny Larue, Joseph Bellier, Pierre De Mey and Guilhem Candille for helpful discussions on the PF inflation and CRPS decomposition.

https://doi.org/10.5194/gmd-2020-130
Preprint. Discussion started: 10 July 2020


Geoscientific Model Development Discussions

References

Aalstad, K., Westermann, S., Schuler, T. V., Boike, J., and Bertino, L.: Ensemble-based assimilation of fractional snow-covered area satellite retrievals to estimate the snow distribution at Arctic sites, The Cryosphere, 12, https://doi.org/10.5194/tc-12-247-2018, https://doi.org/10.5194%2Ftc-12-247-2018, 2018.

Albergel, C., Munier, S., Leroux, D. J., Dewaele, H., Fairbairn, D., Barbu, A. L., Gelati, E., Dorigo, W., Faroux, S., Meurey, C., et al.: Sequential assimilation of satellite-derived vegetation and soil moisture products using SURFEX_v8. 0: LDAS-Monde assessment over the Euro-Mediterranean area, Geoscientific Model Development, 10, 3889–3912, 2017.

Bengtsson, T., Bickel, P., Li, B., et al.: Curse-of-dimensionality revisited: Collapse of the particle filter in very large scale systems, in: Probability and statistics: Essays in honor of David A. Freedman, pp. 316–334, Institute of Mathematical Statistics, 2008.

Buehner, M.: Ensemble-derived stationary and flow-dependent background-error covariances: Evaluation in a quasi-operational NWP setting, Quarterly Journal of the Royal Meteorological Society: A journal of the atmospheric sciences, applied meteorology and physical oceanography, 131, 1013–1043, 2005.

Cantet, P., Boucher, M., Lachance-Coutier, S., Turcotte, R., and Fortin, V.: Using a particle filter to estimate the spatial distribution of the snowpack water equivalent, Journal of Hydrometeorology, 20, 577–594, 2019.

Carmagnola, C. M., Morin, S., Lafaysse, M., Domine, F., Lesaffre, B., Lejeune, Y., Picard, G., and Arnaud, L.: Implementation and evaluation of prognostic representations of the optical diameter of snow in the SURFEX/ISBA-Crocus detailed snowpack model, The Cryosphere, 8, 417–437, https://doi.org/10.5194/tc-8-417-2014, 2014.

Charrois, L., Cosme, E., Dumont, M., Lafaysse, M., Morin, S., Libois, Q., and Picard, G.: On the assimilation of optical reflectances and snow depth observations into a detailed snowpack model, The Cryosphere, 10, 1021–1038, https://doi.org/10.5194/tc-10-1021-2016, 2016.

Clark, M. P., Nijssen, B., Lundquist, J. D., Kavetski, D., Rupp, D. E., Woods, R. A., Freer, J. E., Gutmann, E. D., Wood, A. W., Brekke, L. D., et al.: A unified approach for process-based hydrologic modeling: 1. Modeling concept, Water Resources Research, 51, 2498–2514, 2015.

Cluzet, B., Revuelto, J., Lafaysse, M., Tuzet, F., Cosme, E., Picard, G., Arnaud, L., and Dumont, M.: Towards the assimilation of satellite reflectance into semi-distributed ensemble snowpack simulations, Cold Regions Science and Technology, 170, 102 918, 2020.

Davaze, L., Rabatel, A., Arnaud, Y., Sirguey, P., Six, D., Letreguilly, A., and Dumont, M.: Monitoring glacier albedo as a proxy to derive summer and annual surface mass balances from optical remote-sensing data, The Cryosphere, 12, 271–286, https://doi.org/10.5194/tc-12-271-2018, https://www.the-cryosphere.net/12/271/2018/, 2018.

de Magalhães, N., Evangelista, H., Condom, T., Rabatel, A., and Ginot, P.: Amazonian Biomass Burning Enhances Tropical Andean Glaciers Melting, Scientific reports, 9, 1–12, 2019.

Doucet, A., De Freitas, N., and Gordon, N.: An introduction to sequential Monte Carlo methods, in: Sequential Monte Carlo methods in practice, pp. 472–474, Springer, 2001.

Dozier, J., Green, R. O., Nolin, A. W., and Painter, T. H.: Interpretation of snow properties from imaging spectrometry, Remote Sensing of Environment, 113, S25–S37, 2009.

Durand, Y., Brun, E., Mérindol, L., Guyomarc'h, G., Lesaffre, B., and Martin, E.: A meteorological estimation of relevant parameters for snow models, Ann. Glaciol., 18, 65–71, 1993.

Essery, R., Morin, S., Lejeune, Y., and Bauduin-Ménard, C.: A comparison of 1701 snow models using observations from an alpine site, Adv. Water Res., 55, 131–148, https://doi.org/10.1016/j.advwatres.2012.07.013, 2013.

Evensen, G.: The ensemble Kalman filter: Theoretical formulation and practical implementation, Ocean dynamics, 53, 343–367, 2003.

https://doi.org/10.5194/gmd-2020-130
Preprint. Discussion started: 10 July 2020

Farchi, A. and Bocquet, M.: Comparison of local particle filters and new implementations, Nonlinear Processes in Geophysics, 25, 765–807, 2018.

Fiddes, J., Aalstad, K., and Westermann, S.: Hyper-resolution ensemble-based snow reanalysis in mountain regions using clustering, Hydrology and Earth System Sciences, 23, 4717–4736, 2019.

Gordon, N. J., Salmond, D. J., and Smith, A. F.: Novel approach to nonlinear/non-Gaussian Bayesian state estimation, in: IEE Proceedings F (Radar and Signal Processing), vol. 140, pp. 107–113, IET, 1993.

Hamill, T. M., Whitaker, J. S., and Snyder, C.: Distance-dependent filtering of background error covariance estimates in an ensemble Kalman filter, Monthly Weather Review, 129, 2776–2790, 2001.

Hersbach, H.: Decomposition of the continuous ranked probability score for ensemble prediction systems, Weather and Forecasting, 15, 559–570, 2000.

Houtekamer, P. L. and Mitchell, H. L.: Data assimilation using an ensemble Kalman filter technique, Monthly Weather Review, 126, 796–811, 1998.

Josse, B., Simon, P., and Peuch, V.-H.: Radon global simulations with the multiscale chemistry and transport model MOCAGE, Tellus B: Chemical and Physical Meteorology, 56, 339–356, 2004.

Kitagawa, G.: Monte Carlo filter and smoother for non-Gaussian nonlinear state space models, Journal of computational and graphical statistics, 5, 1–25, 1996.

Kokhanovsky, A., Lamare, M., Danne, O., Brockmann, C., Dumont, M., Picard, G., Arnaud, L., Favier, V., Jourdain, B., Le Meur, E., et al.: Retrieval of snow properties from the Sentinel-3 Ocean and Land Colour Instrument, Remote Sensing, 11, 2280, 2019.

Krinner, G., Derksen, C., Essery, R., Flanner, M., Hagemann, S., Clark, M., Hall, A., Rott, H., Brutel-Vuilmet, C., Kim, H., et al.: ESM-SnowMIP: assessing snow models and quantifying snow-related climate feedbacks, Geoscientific Model Development, 11, 5027–5049, 2018.

Lafaysse, M., Morin, S., Coléou, C., Vernay, M., Serça, D., Besson, F., Willemet, J.-M., Giraud, G., and Durand, Y.: Toward a new chain of models for avalanche hazard forecasting in French mountain ranges, including low altitude mountains, in: Proceedings of the International Snow Science Workshop - Grenoble and Chamonix, pp. 162–166, 2013.

Lafaysse, M., Cluzet, B., Dumont, M., Lejeune, Y., Vionnet, V., and Morin, S.: A multiphysical ensemble system of numerical snow modelling, The Cryosphere, 11, 1173–1198, https://doi.org/10.5194/tc-11-1173-2017, https://www.the-cryosphere.net/11/1173/2017/, 2017.

Lahoz, B. K. W. and Menard, R.: Data assimilation, Springer, 2010.

Lamare, M., Picard, G., Arnaud, L., Tuzet, F., Larue, F., Delcourt, C., and Dumont, M.: Simulating Optical Top-Of-Atmosphere Radiance Satellite Images over Snow-Covered Rugged Terrain, IEEE Transactions on geoscience and remote sensing, in prep, 2020.

Largeron, C., Dumont, M., Morin, S., Boone, A., Lafaysse, M., Metref, S., Cosme, E., Jonas, T., Winstral, A., and Margulis, S. A.: Toward snow estimation in mountains areas using modern data assimilation methods: A review, Frontiers in Earth Science, submitted, 2020.

Larue, F., Royer, A., Sève, D. D., Roy, A., and Cosme, E.: Assimilation of passive microwave AMSR-2 satellite observations in a snowpack evolution model over northeastern Canada, Hydrology and Earth System Sciences, 22, 5711–5734, 2018.

Libois, Q., Picard, G., France, J., Arnaud, L., Dumont, M., Carmagnola, C. M., and King, M.: Influence of grain shape on light penetration in snow, The Cryosphere, 7, 1803–1818, https://doi.org/10.5194/tc-7-1803-2013, 2013.

Libois, Q., Picard, G., Arnaud, L., Dumont, M., Lafaysse, M., Morin, S., and Lefebvre, E.: Summertime evolution of snow specific surface area close to the surface on the Antarctic Plateau, The Cryosphere, 9, 2383–2398, https://doi.org/10.5194/tc-9-2383-2015, 2015.

Liu, J. S. and Chen, R.: Blind deconvolution via sequential imputations, Journal of the american statistical association, 90, 567–576, 1995.

https://doi.org/10.5194/gmd-2020-130
Preprint. Discussion started: 10 July 2020

Magnusson, J., Gustafsson, D., Hüsler, F., and Jonas, T.: Assimilation of point SWE data into a distributed snow cover model comparing two contrasting methods, Water resources research, 50, 7816–7835, 2014.

Magnusson, J., Winstral, A., Stordal, A. S., Essery, R., and Jonas, T.: Improving physically based snow simulations by assimilating snow depths using the particle filter, Water Resources Research, 53, 1125–1143, 2017.

Mankin, J. S., Viviroli, D., Singh, D., Hoekstra, A. Y., and Diffenbaugh, N. S.: The potential for snow to supply human water demand in the present and future, Environmental Research Letters, 10, 114 016, 2015.

Margulis, S. A., Fang, Y., Li, D., Lettenmaier, D. P., and Andreadis, K.: The Utility of Infrequent Snow Depth Images for Deriving Continuous Space-Time Estimates of Seasonal Snow Water Equivalent, Geophysical Research Letters, 46, 5331–5340, 2019.

Mary, A., Dumont, M., Dedieu, J.-P., Durand, Y., Sirguey, P., Milhem, H., Mestre, O., Negi, H. S., Kokhanovsky, A. A., Lafaysse, M., and Morin, S.: Intercomparison of retrieval algorithms for the specific surface area of snow from near-infrared satellite data in mountainous terrain, and comparison with the output of a semi-distributed snowpack model, The Cryosphere, 7, 741–761, https://doi.org/10.5194/tc-7-741-2013, 2013.

Masson, T., Dumont, M., Mura, M. D., Sirguey, P., Gascoin, S., Dedieu, J.-P., and Chanussot, J.: An Assessment of Existing Methodologies to Retrieve Snow Cover Fraction from MODIS Data, Remote Sensing, 10, 619, 2018.

Masson, V., Le Moigne, P., Martin, E., Faroux, S., Alias, A., Alkama, R., Belamari, S., Barbu, A., Boone, A., Bouyssel, F., Brousseau, P., Brun, E., Calvet, J.-C., Carrer, D., Decharme, B., Delire, C., Donier, S., Essaouini, K., Gibelin, A.-L., Giordani, H., Habets, F., Jidane, M., Kerdraon, G., Kourzeneva, E., Lafaysse, M., Lafont, S., Lebeaupin Brossier, C., Lemonsu, A., Mahfouf, J.-F., Marguinaud, P., Mokhtari, M., Morin, S., Pigeon, G., Salgado, R., Seity, Y., Taillefer, F., Tanguy, G., Tulet, P., Vincendon, B., Vionnet, V., and Voldoire, A.: The SURFEXv7.2 land and ocean surface platform for coupled or offline simulation of Earth surface variables and fluxes, Geoscientific Model Development, 6, 929–960, https://doi.org/10.5194/gmd-6-929-2013, 2013.

Matheson, J. E. and Winkler, R. L.: Scoring rules for continuous probability distributions, Management science, 22, 1087–1096, 1976.

Morin, S., Horton, S., Techel, F., Bavay, M., Coléou, C., Fierz, C., Gobiet, A., Hagenmuller, P., Lafaysse, M., Ližar, M., Mitterer, C., Monti, F., Müller, K., Olefs, M., Snook, J. S., van Herwijnen, A., and Vionnet, V.: Application of physical snowpack models in support of operational avalanche hazard forecasting: A status report on current implementations and prospects for the future, Cold Regions Science and Technology, 170, 102 910, https://doi.org/https://doi.org/10.1016/j.coldregions.2019.102910, http://www.sciencedirect.com/science/article/pii/S0165232X19302071, 2020.

Penny, S. G. and Miyoshi, T.: A local particle filter for high-dimensional geophysical systems, Nonlinear Processes in Geophysics, 23, 391, 2016.

Piazzi, G., Thirel, G., Campo, L., and Gabellani, S.: A particle filter scheme for multivariate data assimilation into a point-scale snowpack model in an Alpine environment, The Cryosphere, 12, 2287–2306, 2018.

Pomeroy, J. W., Fang, X., and Marks, D. G.: The cold rain-on-snow event of June 2013 in the Canadian Rockies—Characteristics and diagnosis, Hydrological Processes, 30, 2899–2914, 2016.

Poterjoy, J.: A localized particle filter for high-dimensional nonlinear systems, Monthly Weather Review, 144, 59–76, 2016.

Poterjoy, J. and Anderson, J. L.: Efficient assimilation of simulated observations in a high-dimensional geophysical system using a localized particle filter, Monthly Weather Review, 144, 2007–2020, 2016.

Poterjoy, J., Wicker, L., and Buehner, M.: Progress toward the application of a localized particle filter for numerical weather prediction, Monthly Weather Review, 147, 1107–1126, 2019.

https://doi.org/10.5194/gmd-2020-130
Preprint. Discussion started: 10 July 2020

Raleigh, M. S., Lundquist, J. D., and Clark, M. P.: Exploring the impact of forcing error characteristics on physically based snow simulations within a global sensitivity analysis framework, Hydrol. Earth Syst. Sci., 19, 3153–3179, https://doi.org/10.5194/hess-19-3153-2015, 2015.

Revuelto, J., Lecourt, G., Lafaysse, M., Zin, I., Charrois, L., Vionnet, V., Dumont, M., Rabatel, A., Six, D., Condom, T., et al.: Multi-Criteria Evaluation of Snowpack Simulations in Complex Alpine Terrain Using Satellite and In Situ Observations, Remote Sensing, 10, 1171, 2018.

Richter, B., van Herwijnen, A., Rotach, M. W., and Schweizer, J.: Sensitivity of modeled snow stability data to meteorological input uncertainty, Natural Hazards and Earth System Sciences Discussions, 2020, 1–25, https://doi.org/10.5194/nhess-2019-433, https://www.nat-hazards-earth-syst-sci-discuss.net/nhess-2019-433/, 2020.

Sabatier, T., Largeron, Y., Paci, A., Lac, C., Rodier, Q., Canut, G., and Masson, V.: Semi-idealized simulations of wintertime flows and pollutant transport in an alpine valley: Passive tracer tracking (Part II), Quarterly Journal of the Royal Meteorological Society, n/a, https://doi.org/10.1002/qj.3710, https://rmets.onlinelibrary.wiley.com/doi/abs/10.1002/qj.3710, 2020.

Shaw, T. E., Gascoin, S., Mendoza, P. A., Pellicciotti, F., and McPhee, J.: Snow depth patterns in a high mountain Andean catchment from satellite optical tri-stereoscopic remote sensing, Water Resources Research, 2019.

Snyder, C., Bengtsson, T., Bickel, P., and Anderson, J.: Obstacles to high-dimensional particle filtering, Monthly Weather Review, 136, 4629–4640, 2008.

Stigter, E. E., Wanders, N., Saloranta, T. M., Shea, J. M., Bierkens, M. F., and Immerzeel, W. W.: Assimilation of snow cover and snow depth into a snow model to estimate snow water equivalent and snowmelt runoff in a Himalayan catchment, The Cryosphere, 11, 1647–1664, 2017.

Tuzet, F., Dumont, M., Lafaysse, M., Picard, G., Laurent, A., Voisin, D., Lejeune, Y., Charrois, L., Nabat, P., and Morin, S.: A multilayer physically based snowpack model simulating direct and indirect radiative impacts of light-absorbing impurities in snow, The Cryosphere, 11, 2633, 2017.

Van Leeuwen, P. J.: Particle filtering in geophysical systems, Monthly Weather Review, 137, 4089–4114, 2009.

Vernay, M., Lafaysse, M., Merindol, L., Giraud, G., and Morin, S.: Ensemble Forecasting of snowpack conditions and avalanche hazard, Cold. Reg. Sci. Technol., 120, 251–262, https://doi.org/10.1016/j.coldregions.2015.04.010, 2015.

Vetterling, W. T., Teukolsky, S. A., Press, W. H., and Flannery, B. P.: Numerical recipes in Fortran the art of scientific computing, Cambridge University Press, 1992.

Veyssière, G., Karbou, F., Morin, S., Lafaysse, M., and Vionnet, V.: Evaluation of Sub-Kilometric Numerical Simulations of C-Band Radar Backscatter over the French Alps against Sentinel-1 Observations, Remote Sensing, 11, 8, 2019.

Vionnet, V., Brun, E., Morin, S., Boone, A., Martin, E., Faroux, S., Le-Moigne, P., and Willemet, J.-M.: The detailed snowpack scheme Crocus and its implementation in SURFEX v7.2, Geosci. Model. Dev., 5, 773–791, https://doi.org/10.5194/gmd-5-773-2012, 2012.

Vionnet, V., Dombrowski-Etchevers, I., Lafaysse, M., Quéno, L., Seity, Y., and Bazile, E.: Numerical weather forecasts at kilometer scale in the French Alps : evaluation and applications for snowpack modelling, J. Hydrometeor., https://doi.org/http://dx.doi.org/10.1175/JHM-D-15-0241.1, 2016.

Warren, S. G.: Can black carbon in snow be detected by remote sensing?, J. Geophys. Res., 118, 779–786, https://doi.org/10.1029/2012JD018476, 2013.

Wayand, N. E., Marsh, C. B., Shea, J. M., and Pomeroy, J. W.: Globally scalable alpine snow metrics, Remote Sensing of Environment, 213, 61–72, 2018.

https://doi.org/10.5194/gmd-2020-130
Preprint. Discussion started: 10 July 2020

Winstral, A., Magnusson, J., Schirmer, M., and Jonas, T.: The Bias-Detecting Ensemble: A New and Efficient Technique for Dynamically Incorporating Observations Into Physics-Based, Multilayer Snow Models, Water Resources Research, 55, 613–631, 2019.

Wright, P., Bergin, M., Dibb, J., Lefer, B., Domine, F., Carman, T., Carmagnola, C., Dumont, M., Courville, Z., Schaaf, C., et al.: Comparing MODIS daily snow albedo to spectral albedo field measurements in Central Greenland, Remote sensing of environment, 140, 118–129, 2014.

Würzer, S., Jonas, T., Wever, N., and Lehning, M.: Influence of initial snowpack properties on runoff formation during rain-on-snow events, Journal of hydrometeorology, 17, 1801–1815, 2016.

https://doi.org/10.5194/gmd-2020-130
Preprint. Discussion started: 10 July 2020

Geoscientific Model Development Discussions

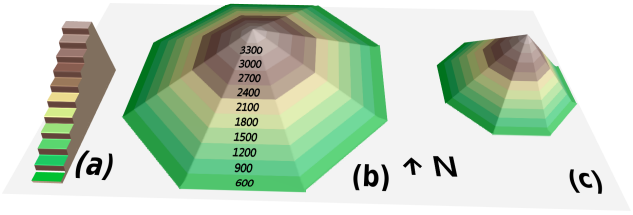

Figure 1. 3D schematic view of the semi-distributed geometry, where the numbers represent the elevation bands altitudes (m). From left to right, the three different mountains represent the flat, 20^{o} and 40^{o} degrees slopes.

https://doi.org/10.5194/gmd-2020-130
Preprint. Discussion started: 10 July 2020

Geoscientific Model Development
Discussions
Open Access
EGU

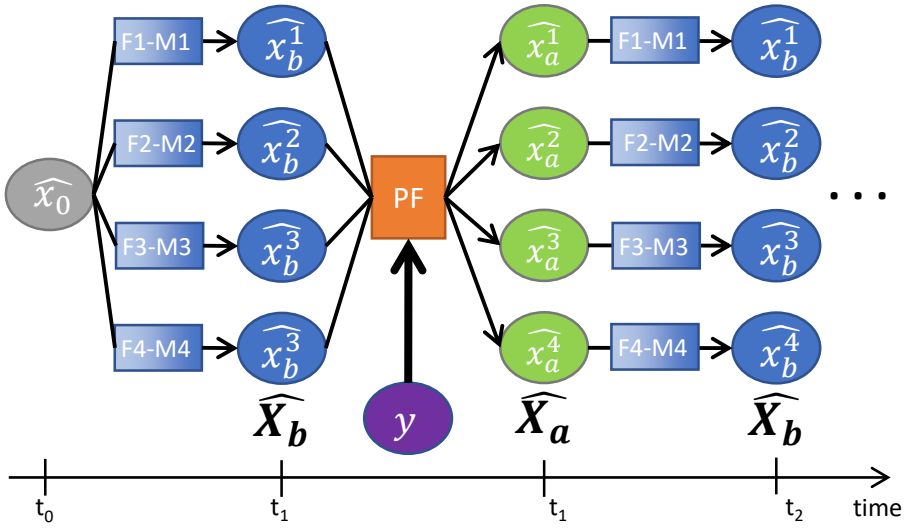

Figure 2. Workflow of CrocO ensemble data assimilation system with 4 members. $\widehat{x_0}$: initial state at time t_0, Fi: forcing, Mi: ESCROC member, $\widehat{X_b}$: background state, $\widehat{x_b^i}$: background particles, $\widehat{X_a}$: analysis, $\widehat{x_a^i}$: analysis particles, y: observation, t_1 and t_2: observation dates.

https://doi.org/10.5194/gmd-2020-130
Preprint. Discussion started: 10 July 2020

Geoscientific Model Development Discussions
Open Access
EGU

PF Algorithm	N_e	inflation	N^*_{eeff}	HS σ_o^2 (m^2)
rlocal	40	on	7	1.0×10^{-2}
global	40	on	7	1.0×10^{-2}
klocal	40	on (if k=1)	7	5.0×10^{-2}

Table 1. setup of the Snow depth assimilation experiment.

https://doi.org/10.5194/gmd-2020-130
Preprint. Discussion started: 10 July 2020

Geoscientific Model Development Discussions
Open Access
EGU

PF Algorithm	N_e	inflation	N^*_{eeff}	B4 σ_o^2	B5 σ_o^2
rlocal	40	on	7	5.6×10^{-4}	2.0×10^{-3}
global	40	on	7	5.6×10^{-4}	2.0×10^{-3}
klocal	40	on (if k=1)	7	2.8×10^{-3}	1.0×10^{-2}

Table 2. setup of the second reflectance assimilation experiment.

https://doi.org/10.5194/gmd-2020-130
Preprint. Discussion started: 10 July 2020

Geoscientific Model Development Discussions
Open Access
EGU

PF Algorithm	N_e	inflation	N^*_{eeff}	B4 σ_o^2	B5 σ_o^2
rlocal	160	on	25	5.6×10^{-4}	2.0×10^{-3}
global	160	on	25	5.6×10^{-4}	2.0×10^{-3}
klocal	160	on (if k=1)	25	2.8×10^{-3}	1.0×10^{-2}

Table 3. setup of the second reflectance assimilation experiment.

https://doi.org/10.5194/gmd-2020-130
Preprint. Discussion started: 10 July 2020

Geoscientific Model Development
Discussions
Open Access
EGU

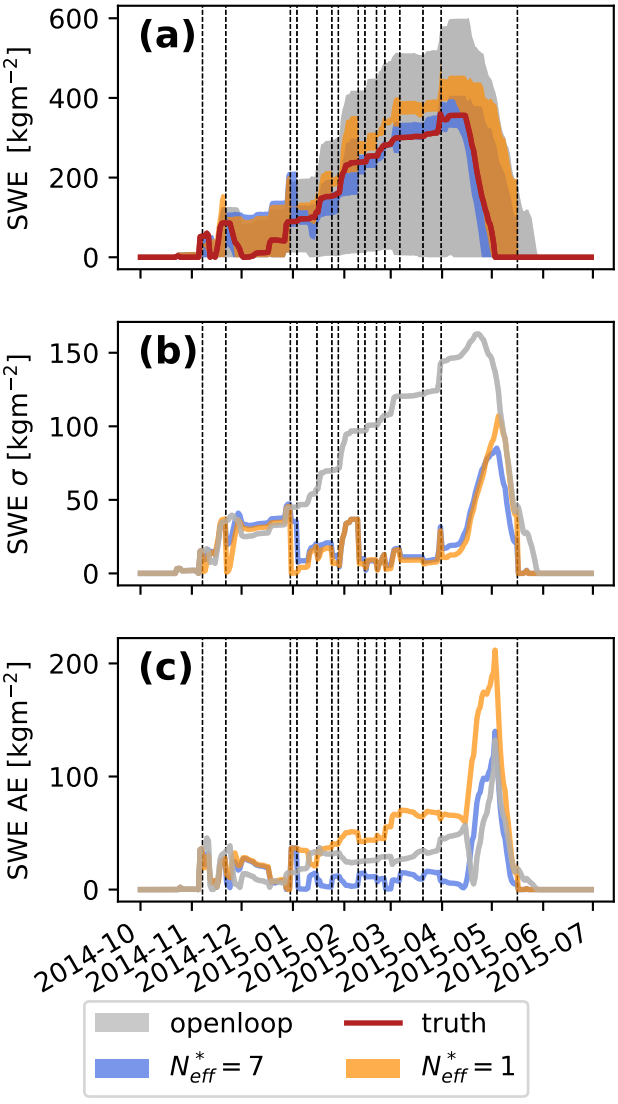

Figure 3. Impact of the inflation ($N^*_{\text{eff}} = 7$) versus no inflation ($N^*_{\text{eff}} = 1$) in the 1800_N_40 topographic class (not observed), when assimilating HS of 2015_q80 with the *global* PF. (a) SWE minimum-maximum envelopes as a function of time, (b) spread and (c) RMSE. Dashed lines represent the assimilation dates.

https://doi.org/10.5194/gmd-2020-130
Preprint. Discussion started: 10 July 2020

Geoscientific Model Development Discussions

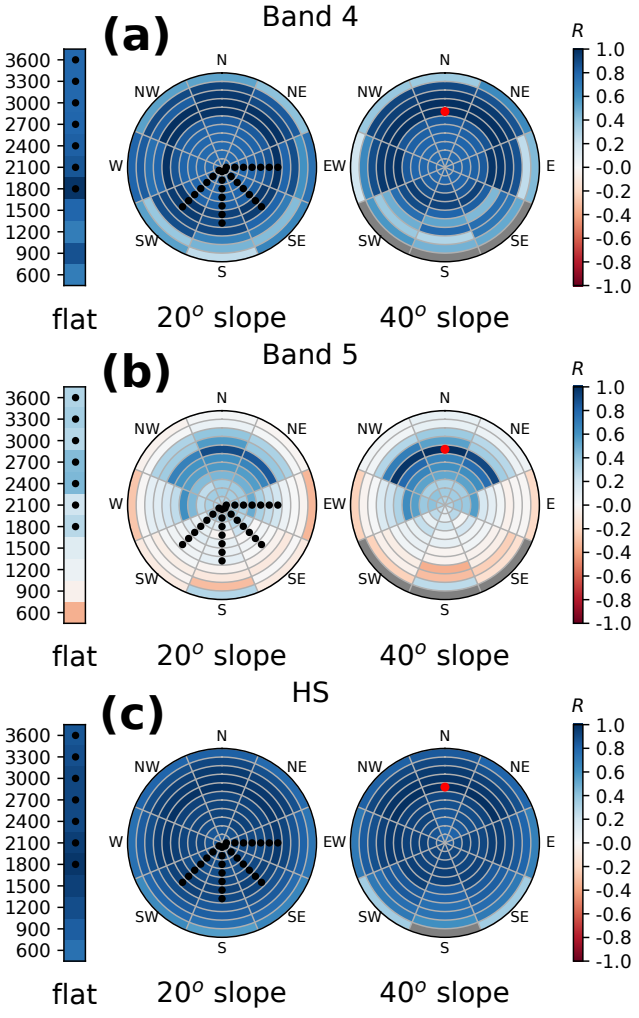

Figure 4. 2015, February 20th openloop (40 members) Pearson correlations between the domain points and the 1800_N_40 topographic class (red dot), in Band 4 (a), Band 5 (b) and HS (c). Left bars show the flat topographic classes in the associated elevation bands, while pie plots show the 20^o and 40^o slope topographic classes, as depicted in Fig. 1. Black dots the denote observed classes.

https://doi.org/10.5194/gmd-2020-130
Preprint. Discussion started: 10 July 2020

Geoscientific Model Development
Discussions
Open Access
EGU

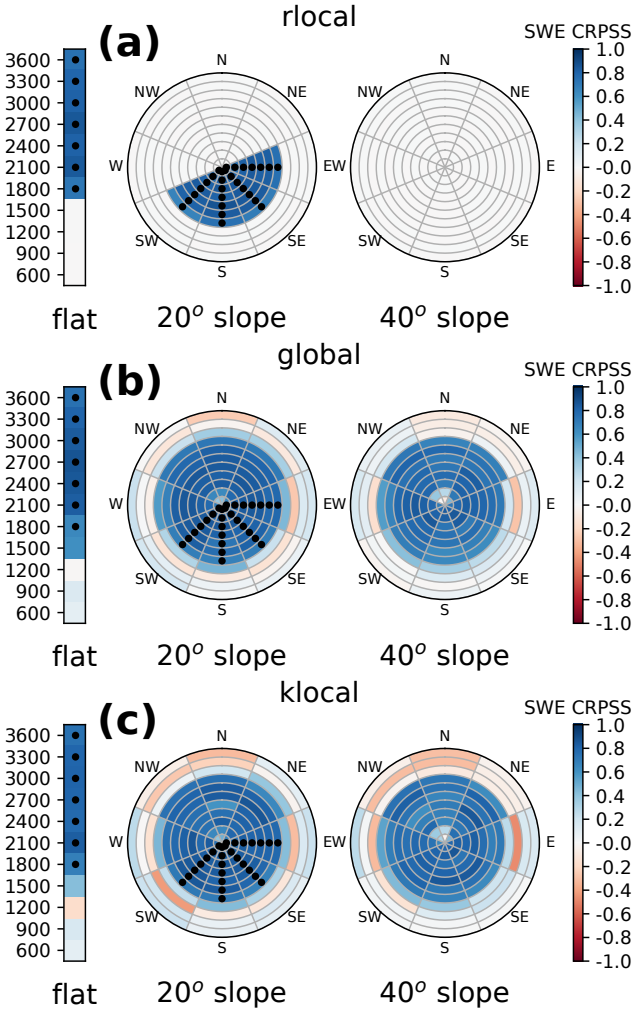

Figure 5. CRPS Skill Score of SWE for the *rlocal* (a), *global* (b) and *klocal* (c) algorithms assimilating the HS of 2013_p20 synthetic member. The score is computed on the whole snow season for each topographic class. Black dots denote the observed classes.

https://doi.org/10.5194/gmd-2020-130
Preprint. Discussion started: 10 July 2020

Geoscientific Model Development Discussions
Open Access
EGU

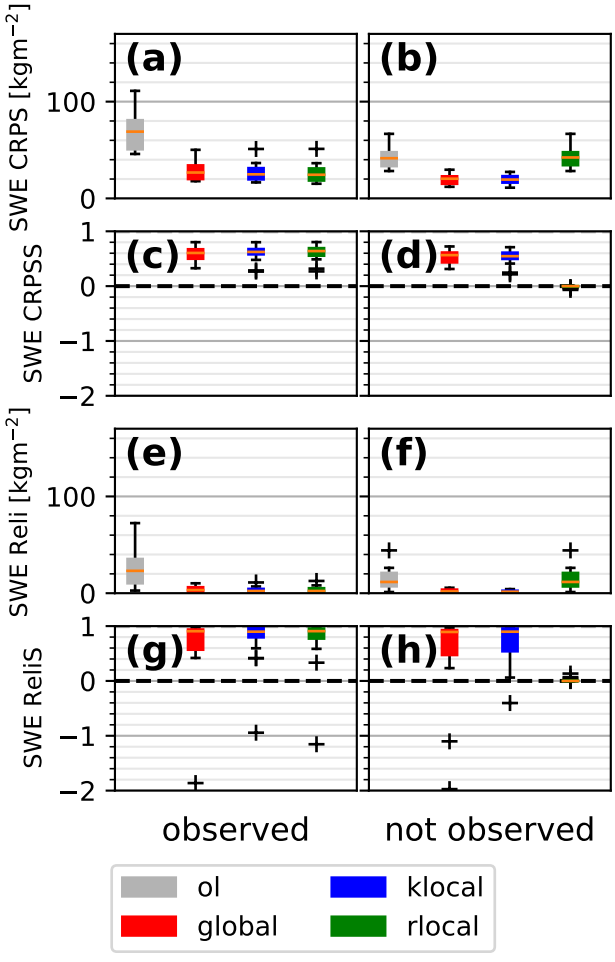

Figure 6. Boxplots of SWE CRPS (a,b) and Reli (e,f) for the different algorithms for the 16 different synthetic members, separated between observed (left column) and not observed (right panel) classes. Panels (c,d) and (g,h) show the associated Skill Scores.

https://doi.org/10.5194/gmd-2020-130
Preprint. Discussion started: 10 July 2020

Geoscientific Model Development
Discussions
Open Access
EGU

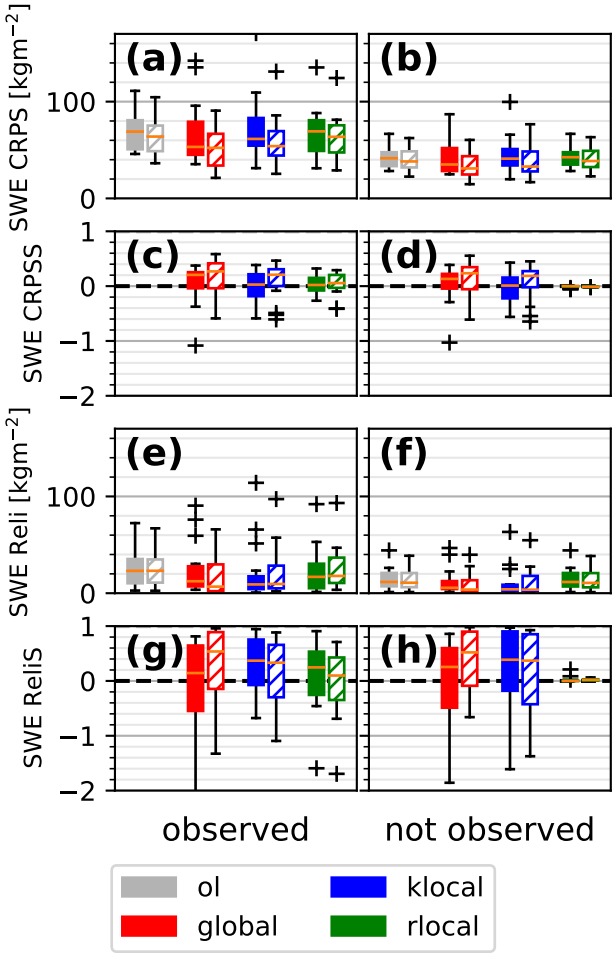

Figure 7. Same as Fig. 6 for reflectance with 40 members (filled) and 160 members (hatched).

https://doi.org/10.5194/gmd-2020-130
Preprint. Discussion started: 10 July 2020

Geoscientific Model Development
Discussions
Open Access
EGU

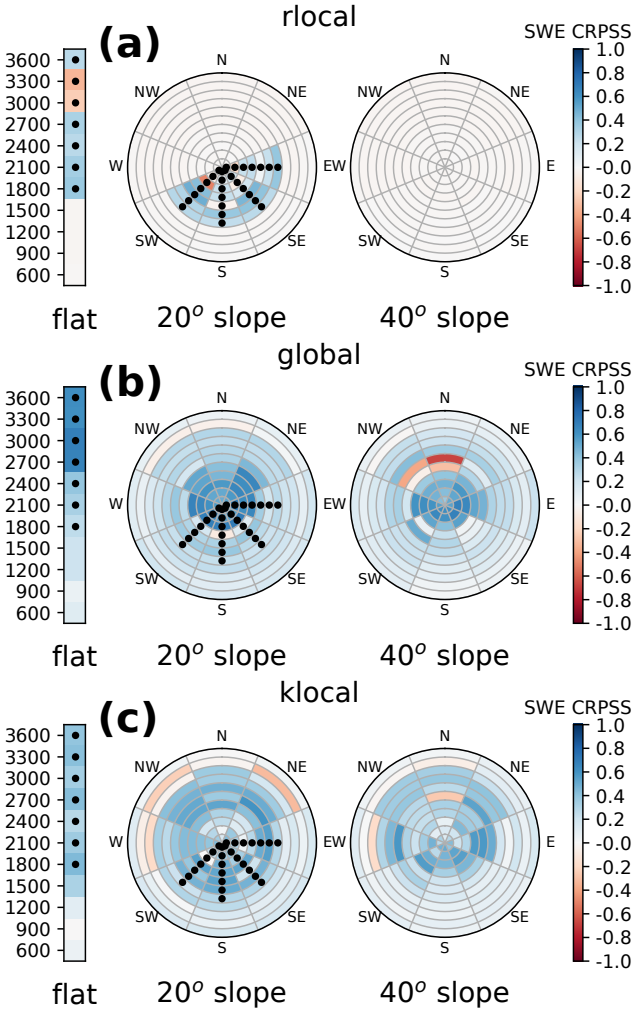

Figure 8. Same as Fig. 5 for the assimilation of the reflectance of 2016_p60 member.

https://doi.org/10.5194/gmd-2020-130
Preprint. Discussion started: 10 July 2020

Geoscientific Model Development
Discussions
Open Access
EGU

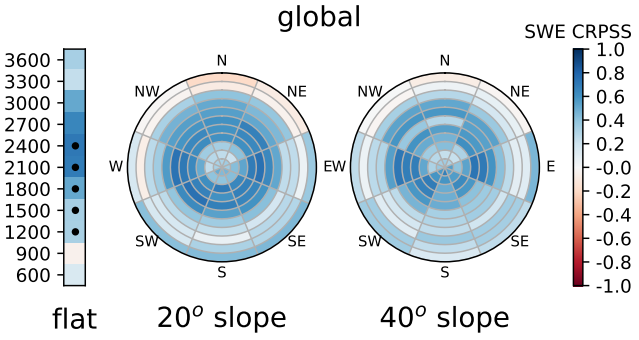

Figure 9. Same as Fig. 5 for the assimilation of HS of 2016_p60 member in the 1200-2400 m flat classes.